Journal of Materials Chemistry A

Accepted Manuscript

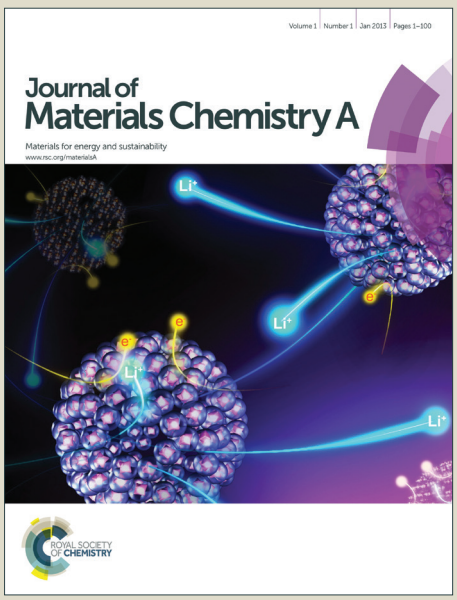

ROYAL SOCIETY OF CHEMISTRY

www.rsc.org/materialsA

Cite this: DOI: 10.1039/c0xx00000x

www.rsc.org/xxxxxx

COMMUNICATION

Sulfur-infiltrated three-dimensional graphene-like material with hierarchical pores for highly stable lithium-sulfur batteries

Yunyong Li, Zesheng Li, Qinwei Zhang, and Pei Kang Shen*

Received (in XXX, XXX) Xth XXXXXXXXX 20XX, Accepted Xth XXXXXXXXX 20XX

DOI: 10.1039/b000000x

A rational design and synthesis of sulfur-carbon nanocomposites by infiltrating into 3D graphene-like material (GlM) with hierarchical pores has been achieved for the first time and such 3D GlM/S nanocomposite shows a highly stable capacity and reversible high rate charge/discharge performance.

Lithium-sulfur (Li-S) batteries are considered to be promising choice for the next generation high-energy rechargeable batteries due to their high theoretical energy density of 2567 Wh kg^{-1}, calculated on the basis of the Li anode (~3860 mAh g^{-1}) and the S cathode (~1675 mAh g^{-1})[1-3]. Additionally, Li-S batteries are conducted with abundant and nontoxic sulfur that is a common by-product of the petroleum refining process, making it attractive for large-scale practical applications.[4, 5] Despite these significant advantages, large-scale commercial use is still a big challenge.[6] First of all, sulfur is known to suffer from the problem of inherent poor electronic/ionic conductivities, making it severely limits the practical use of sulfur in an electrode.[7] Secondly, the intermediates of the electrochemical reactions, long-chain polysulphides (Li_2S_n, $3<n<8$), is highly soluble in conventional organic electrolytes.[8] The sulfur cathode and lithium anode would be shuttled by dissolved polysulfide ions, causing precipitation of insoluble and insulating Li_2S_2/Li_2S on the surface of the electrodes.[9] This undesirable phenomenon not only results in low Coulombic efficiency and losses active material but also hampers the ionic accessibility of the electrodes.[10, 11] Consequently, low specific capacity and fast capacity fading are commonly found in sulfur cathodes.[12] Thirdly, the obvious volumetric expansion of sulfur occurs during charging process, described by the reaction $S+2Li \rightarrow Li_2S$, since the density of Li_2S is only 1.66 g cm^{-3} which are lower than sulfur (2.03 g cm^{-3}).[5, 13]

To overcome above problems, conducting polymers and carbon have been utilized as matrix for Li-S batteries due to their good electronic conductivity and adsorption capacity.[14, 15] Compared with conducting polymers, carbon materials have higher electronic conductivity and structural stability.[4, 16] In particularly, porous carbon materials can effectively improve the sulfur utilization and restrain the solubility of polysulphides on account of their excellent electronic conductivity, large surface area, and narrow pores that result in a conductive matrix and strong adsorption agent.[7, 17]

An ideal porous carbon matrix for sulfur-carbon composites[4, 18] should include (i) high electronic conductivity to improve the utilization of sulfur, (ii) suitable electrochemical affinity for sulfur to achieve high capacity (in-depth sulfur utilization), (iii) small pores without large outlets to accommodate polysulphides, (iv) large specific surface area to load sufficient sulfur as thin layer, (v) suitable structure of the active material which remains sufficient void volume after sulfur infiltration to accept the liquid electrolyte and (vi) stable framework to sustain the strain generated by the volume changes of the active material during cycling.

Currently, various porous carbons are employed to prepare C/S composites, such as microporous carbon,[19, 20] mesoporous carbon,[21] porous carbon fibres,[22] and graphene.[23, 24] Among these carbonaceous materials, graphene, with a single layer or few layers of graphitic carbon, is regarded as a promising candidate for an ideal porous carbon matrix due to its large theoretical surface area, good electronic conductivity, high electrochemical stability and tuneable surface functionalization for the hydrophobicity/hydrophilicity.[4, 16, 25, 26] However, the exfoliated graphene tends to restack or aggregate due to the strong dangling bonds among individual graphene sheet, resulting in low surface area (down to ≤ 100 m^2 g^{-1}) and thus limiting its many unique properties and practical applications.[4, 16, 25, 26] In addition, although graphene sheets are advantageous for wrapping sulfur because of their large lateral size, good conductivity and the flexible structure. Under ideal conditions, however, graphene sheets conduct ions along the lateral direction making ion conduction across the sheets very difficult. To make graphene fit for Li-S battery applications, many studies on efficient assembly of three-dimensional (3D) macroporous graphene (MG) have been conducted.[26-30] For example, fabricating sandwich-structured graphene-sulfur composites by a thermal annealing[23] or hydrothermal technique,[28] or forming 3D macroporous structured graphene-sulfur composites by a one-pot hydrothermal assembly of graphene and sulfur,[26] or assembling flexible self-supporting graphene-sulfur composites by an *in situ* redox reaction followed by vacuum infiltration.[29] These self-assembled 3D MG can provide interconnected macroporous structures for rapid mass and ion

transport as well as relatively large surface area for large amount of sulfur sequestered to improve the electrochemical performance, especially, the rate capability for Li-S batteries. Unfortunately, these self-assembled 3D MGs were built from graphene oxide or reduced graphene oxide precursor, which have a partly restored graphitic structure and relatively large O/C atomic ratio (including abundant oxygen functional group), thus resulting in relatively insufficient conductivity and stability. Therefore, these self-assembled 3D MG still do not meet the requirements of an ideal porous carbon matrix. In addition, relative to the self-assembled 3D MG, the catalytic routes for 3D MG synthesis have distinct advantages in increasing the conductivity and stability of the graphene materials,[31-35] thus can further improve the utilization of sulfur and rate capability in Li-S batteries. However, these "bottom-up" synthesized 3D MG contain few micropores and small mesopores, thus the sulfur and subsequent lithium polysulfides during the charge/discharge process may be not stably confined after sulfur infusion. Therefore, the phenomenon of the polysulfide dissolution and shuttling in the electrolytes will probably be easy to happen, especially in the case of high sulfur loadings it will probably be more easier to happen, thus maybe result in limited capacity and cycle performance. It is a critical challenge to develop an effective three-dimensional porous graphene-like structured material for stably loading of sulfur layer.

Herein, we report on the rational design and synthesis of new sulfur-carbon nanocomposites by infiltrating sulfur into a 3D graphene-like material (GlM) with hierarchical pores (Fig. S1). The 3D GlM material, synthesized from a ion-exchange resin based technology, combining large pore volume (2.5 cm^3 g^{-1}), high surface area (2700 m^2 g^{-1}), high conductivity (1224 S m^{-1}) and suitable hierarchical pores together, has been used to infuse sulfur which is based on the following considerations. (i) Abundant micro- and mesopores can provide large total pore volume (large surface area) to maximize the loading of sulfur (could be 72.3 wt % S or more) sequestered by 3D GlM, (ii) interconnected micro-, mesopores, and sub-micrometer sized macropores to provide appropriate surfaces and channels to facilitate the sulfur into the interior micro- and mesoporous walls, and preserve fast transport of lithium ions to the sequestered sulfur by ensuring good electrolyte penetration, (iii) 3D porous structure can accommodate the polysulfide in interior pores to minimize lithium polysulfide dissolution and shuttling in the electrolyte, which can enhance the utilization of sulfur to improve the cycle life, and they can also provide stable frame-work to sustain the strain generated by the volume changes of the active material during cycling, and (iv) graphene-like structure can provide excellent electronic conductivity to facilitate good transport of electrons from the poorly conducted sulfur. Used as the cathode material in Li-S secondary batteries, the as-prepared 3D GlM/S nanocomposite (43.6 wt %S) remained 1067 mAh g^{-1} after 300 cycles (at 0.5 C charge/discharge rate), showing a manifest promising electrochemical behavior. The 3D GlM/S nanocomposite with higher S loadings (72.3 wt %S) also remained 854 mAh g^{-1} after 200 cycles, consistent with our goals in the designing of the 3D GlM.

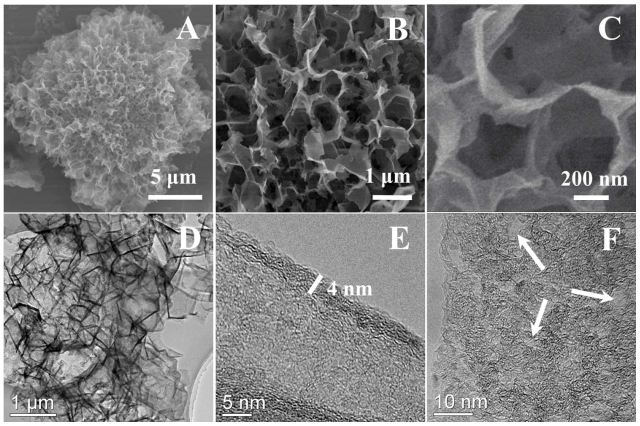

Fig. 1. (A-C) SEM micrographs with different magnifications and (D) low-resolution TEM image of 3D GlM, (E) the high-resolution TEM of the edge of the graphene-like wall and (F) the mesoporous texture of the graphene-like wall. The presence of the small size mesopores ranging from 2 to 7 nm are clearly observed (some are indicated by the white arrows).

The 3D GlM was synthesized a one-step ion-exchange/activation combination method using an inexpensive metal ion exchanged resin as a carbon precursor (see experimental section for details, step I in Fig. S1), Fig. 1A and 1B show the typical scanning electron microscopic (SEM) micrographs of the 3D GlM sample, revealing the formation of a unique interconnected 3D porous network. The magnified SEM micrograph exhibits sub-micrometer-sized macropores and thin layer graphene-like walls (Fig. 1C) of 3D GlM. The transmission electron microscopy (TEM) images further confirmed that the material shows an interconnected 3D porous network (Fig. 1D). The thin layer graphene-like wall exhibits generally 4 nm thick and high degree of graphitization (Fig. 1E). Fig. 1F displays many small mesopores ranging from 2 nm to 7 nm on the walls of the 3D GlM, which formed by the activation of KOH. The porosity and surface area of the material can be easily adjusted by change the preparation conditions. Such a highly interconnected porous structure maybe provide an ideal carbon matrix for sulfur loading and encapsulation.

In the second step (step II in Fig. S1), the sulfur impregnation of the 3D GlM was performed by an improved melt-diffusion strategy (see experimental section for details) to facilitate the infusion of sulfur into the carbon structure and achieve better encapsulation of sulfur. A 1:3 mass ratio mixture of 3D GlM to sulfur was prepared by above melt-diffusion process. The sulfur content of the sample was confirmed (Fig. S2 A, pink curve) by thermo-gravimetric analysis (TGA), which is 72.3 wt %S. The 3D GlM/S nanocomposite (72.3 wt %S) shows similar SEM morphology of interconnected 3D porous network compared with the pristine 3D GlM sample (Fig. 1A). No discernible sulfur particles were found on the carbon surface, suggesting the uniform dispersion of sulfur onto the carbon matrix. The TEM image of 3D GlM/S nanocomposite (72.3 wt %S) (Fig. 2B) also exhibits the similar continuous 3D porous network as SEM micrograph. In the high-resolution TEM image, it also

showed the 3D porous structure without discernible sulfur particles plugging (Fig. 2C). The TEM elemental mapping (Fig. 2C_1 and 2C_2) of the 3D porous structure demonstrated that the sulfur uniformly impregnated onto the 3D macroporous walls, which was consistent with the results of elemental mapping of graphene-like walls (Fig. S3).

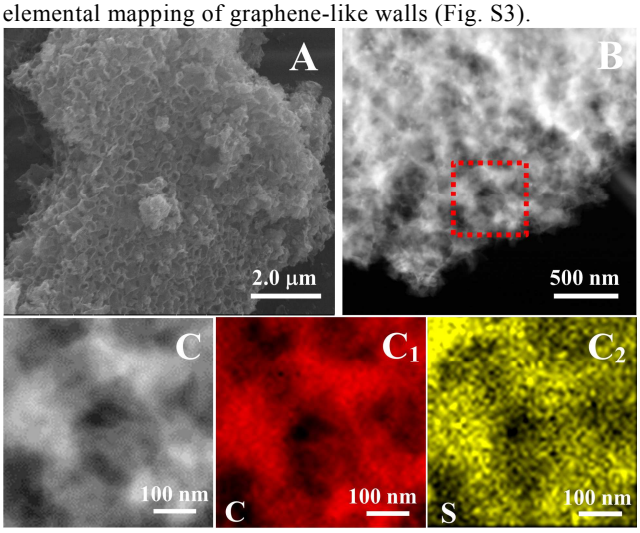

Fig. 2. (A) SEM micrograph and TEM image (B) as well as TEM elemental mapping (C) of carbon (C_1) and sulfur (C_2) corresponding to the outlined area by the red square in (B) for the 3D GlM/S (72.3 wt %S) sample.

To further evidence the impregnation of sulfur on the porous structure of 3D GlM, nitrogen adsorption/desorption experiments were conducted to investigate the pore-size characteristics of 3D GlM before and after sulfur infusion. Other two 3D GlM/S nanocomposities with low sulfur contents were also prepared by the same melt-diffusion method to better understand the process of sulfur infusion. The sulfur contents of the two samples were confirmed (Fig. S2 A) by TGA: 43.6 wt %S (red curve) and 62.8 wt %S (blue curve), respectively. Fig. 3A shows the isotherms of the 3D GlM before and after sulfur infusion. The isotherm of the 3D GlM (Fig. 3A, black circle curve) exhibits combined characteristics of type II/IV,[37] with a Brunauer-Emmett-Teller (BET) surface area of 2700 m^2 g^{-1}, a total pore volume of 2.50 cm^3 g^{-1}, about 82.4 % of total pore volume contributed from different size pores under 7 nm. After sulfur infusion into the 3D GlM, the nitrogen sorption isotherms (Fig. 3A) becomes weaker but the hysteresis region becomes less obvious with increased sulfur loading, corresponding to a systematic decrease of the specific surface area and total pore volume. Table S1 summarizes the data. The micro- and mesoporous volumes (2-7 nm) are gradually decreased with the increase in sulfur content, until almost disappear when the sulfur content reaches up to 72.3 wt%. These results demonstrated that sulfur is deeply impregnating into micro- and mesopores (2-7 nm), which is consistent with the TEM mapping results. In addition, the large pore volumes (>7 nm) of the three 3D GlM/S nanocomposites do not exhibit obivious change with increased sulfur loading and keep similar size as that of 3D GlM. The results may be mainly due to that the large amount of sulfur were infused into the micro- and small mesopores (2-7 nm) of 3D GlM, thus the large void pores of the 3D GlM after sulfur infusion were still mainly remained. Moreover, the corresponding density functional theory (DFT) pore size distributions also demonstrate the similar results (Fig. 3B). The 3D GlM exhibits a hierarchical pore distribution with abundant micro- and mesopores. After sulfur infusion, the intensity of the peaks for the micro- and mesopores (2-7 nm) of the 3D GlM becomes broader and smaller with increased sulfur content, until these peaks disappear at the sulfur content of 72.3 wt%, but the peaks of large pores (>7 nm) have no obivious change with increased sulfur loading. Such a hierarchical porous sturcture with interconected micro-, meso- and macropores is favoreble for mass transfer during the charge/discharge processes.

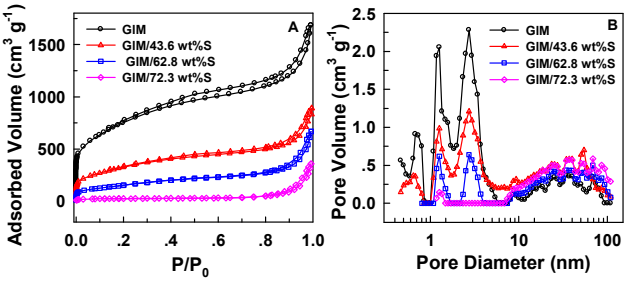

Fig. 3. (A) Nitrogen adsorption/desorption isotherms and (B) DFT pore-size distribution curves of 3D GlM and 3D GlM/S nanocomposites.

The structure of the 3D GlM before and after sulfur infusion was studied by powder X-ray diffraction (XRD) as shown in Fig. S2B. The sharp diffraction peaks denote that sulfur exists in a crystalline state (Fig. S2B, gray curve). The XRD pattern of the 3D GlM shows a relatively sharp peak at 2θ =26.2°, suggesting a high degree of graphitization of the 3D GlM, which is coincident with the result of X-ray photoelectron spectroscopy (XPS) (Fig. S4). By comparison, all of the three 3D GlM/S nanocomposites exhibit only one main peak at 26.2° as that of 3D GlM. This result demonstrated that sulfur existed inside the porous structure of 3D GlM as a highly dispersed amorphous state, which agrees well with the results of the SEM and TEM. In addition, the 3D GlM + 69.7 wt %S sample (made by the mixture of 3D GlM and S, instead of melt-diffusion process, and the sulfur content of 69.7 wt %S was confirmed as shown in Fig. S2A) shows the obvious crystalline sulfur diffraction peaks, demonstrating the existence of numerous bulk or aggregated sulfur without impregnation into 3D GlM. Furthermore, the powder conductivities of the 3D GlM before and after sulfur infusion were also examined by a four-probe method and the results are listed in Table S1. The average powder conductivity of the 3D GlM is about 1224 S m^{-1}, which is more than twice as high as that of the KOH-activated graphene material.[38] Most importantly, all of the powder conductivities of the three 3D GlM/S nanocomposites were very close as its pristine 3D GlM, indicating that the materials still kept excellent electronic transportation after the insulating sulfur doping. This is the evidence that the insulating sulfur uniformly dispersed on the interior porous walls of the 3D GlM as thin layer and remained the electronic

conducting pathways. Such a highly dispersed state in the confined space may generate essential electric contact and restrain the diffusion of the polysulfides. The interconnected pores enable rapid transport of the Li^+ ions during the charge/discharge processes.

To study the electrochemical properties of the 3D GlM/S nanocomposites, the CR2032 coin cells with metallic lithium counter electrode were assembled and evaluated, along with the comparison with 3D GlM + 69.7 wt %S sample. Fig. 4A shows the typical cyclic voltammetric (CV) curves of a 3D GlM/S nanocomposite (72.3 wt %S) electrode in the voltage range of 1.5-3.0 V with a constant scan rate of 0.1 mV s^{-1}. In the first cathodic scan, a pair of sharp reductive peaks at 2.33 and 2.03 V demonstrate that the electrochemical reduction of sulfur substantially occurs in two stages. The first peak (I) at 2.33 V is assigned to a fast kinetic process, involving the reduction of elemental sulfur to long-chain lithium polysulfide (Li_2S_n, $4 \le n < 8$).[6, 17] The second peak (II) at 2.03 V involves the reduction of sulfur in lithium polysulfide to Li_2S_2 and eventually to Li_2S, which is a slower kinetic process than first one and contributes to large proportion of capacity.[17] It is hindered by the sluggishness of the solid state diffusion in the bulk. In the next anodic process, the oxidation peak (III) at 2.36 V is associated with the formation of Li_2S_n ($n>2$).[39] This process continues until lithium polysulfide is completely consumed and the elemental sulfur produced at 2.48 V (IV).[6, 40] Significantly, no obvious changes in the CV peak positions or peak current are observed in next 9 cycles, confirming the electrochemical stability of the 3D GlM/S nanocomposite even at high sulfur content (72.3 wt %S). It also indicated that the porous carbon structure is quite effective in preventing the loss of sulfur into the electrolyte and maintained high utilization of the active sulfur in the redox reactions.

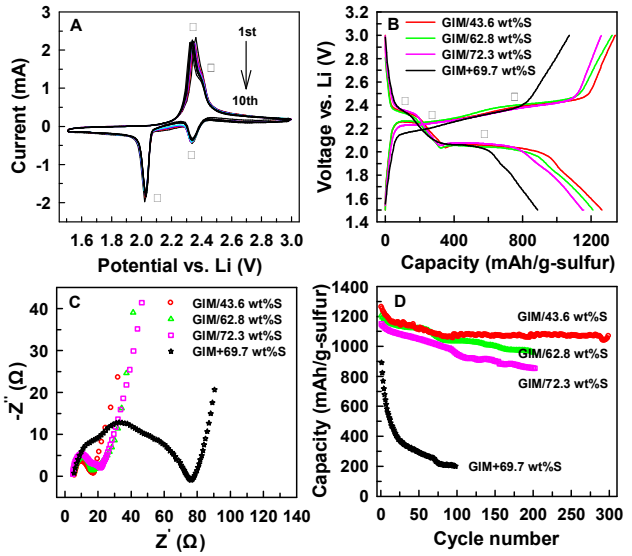

Fig. 4. Electrochemical performances of various cathode materials. (A) Typical CV curves of 3D GlM/S nanocomposite (72.3 wt%S) cathode at a scan rate of 0.1 mV s^{-1}, (B) the galvanostatic charge/discharge profiles for first cycle at a discharge rate of 0.5 C, (C) Nyquist plots after the first cycle and (D) the cycling performance at a discharge rate of 0.5 C.

Fig. 4B exhibits the charge/discharge voltage profiles for the three 3D GlM/S nanocomposites and the 3D GlM+69.7 wt%S sample. It is immediately apparent from this figure that the charge/discharge voltage plateaus, marked as I (2.33 V), II (2.05 V), III (2.31 V), and IV (2.43 V) (Note: due to the charge/discharge voltage plateaus were not very flat, the average values were given), corresponding well to the redox peaks observed in the CV curves. The 3D GlM/S nanocomposite (43.6 wt %S) shows an impressive initial discharge capacity of 1262 mAh g^{-1} at a rate of 0.5 C. For the other evaluated 3D GlM/S nanocomposites, the initial discharge capacity of 62.8 wt %S is commendable at 1211 mAh g^{-1} and of 72.3 wt %S is 1150 mAh g^{-1}, respectively. For comparison, the 3D GlM+69.7 wt %S sample only exhibited the discharge capacity of 890 mAh g^{-1}.

Fig. 4C gives the interfacial charge-transfer resistance of the 3D GlM/S nanocomposites and 3D GlM+69.7 wt %S sample measured by electrochemical impedance spectroscopy (EIS). Surprisingly, the 3D GlM/S nanocomposite (43.6 wt %S) showed a very small semicircle, that is, low charge transfer resistance (R_{ct}) of 12 Ω. It was only 15 Ω for a 3D GlM/S nanocomposite (72.3 wt %S), which is far lower than other reported C/S nanocomposites.[40-43] Such low R_{ct} data of 3D GlM/S nanocomposites are mainly due to two factors. The first one is that the highly dispersed sulfur in interior porous structure of 3D GlM does not block the current pathway, which has been proven by SEM, TEM and XRD measurements. Another one is the high conductivity of the 3D GlM to facilitate fast charge/discharge of the nearby sulfur. In contrast, the 3D GlM+69.7 wt %S sample exhibited a large R_{ct} of 71 Ω. In addition, the R_{ct} values of the 3D GlM/S nanocomposites are hardly changed after 100 cycles compared with the first cycle. While, large change appeared for the 3D GlM+69.7 wt %S sample (Fig. S5). This result indicates that the irreversible deposition and aggregation of insoluble reduction products (Li_2S_2 and Li_2S) on the walls of 3D GlM/S nanocomposites are negligible. It is beneficial to the high-rate capability during long cycling.

The comparative cycling stabilities of three 3D GlM/S nanocomposites and 3D GlM+69.7 wt %S sample at a discharge rate of 0.5 C are given in Fig. 4D. Among the evaluating cathodes, the 3D GlM/S nanocomposite (43.6 wt %S) displayed the best electrochemical performance. It delivered an outstanding initial capacity of 1262 mAh g^{-1} and the capacity retained as high as 1067 mAh g^{-1} (84.5% capacity retention) after 100 cycles and then kept constant in the next 200 cycles. Such a high stability is comparable and/or superior to advanced conventional cathode materials like $LiFePO_4$@C,[44-46] $LiMn_2O_4$/C[47-49] and $LiCoO_2$-based materials.[50-52] Moreover, the energy density of the total 3D GlM/S nanocomposite (containing 43.6 wt %S) is 465 mAh g^{-1}, which is almost three times higher as those of conventional cathode materials (~160 mAh g^{-1}). The bad news is that the average discharge plateau is only 2.03 V, which is lower than those of conventional cathode materials (3.0-3.7 V).[44-52] The 3D GlM/S nanocomposites with higher loadings of sulfur (e.g., 62.8 wt %S and 72.3 wt %S) showed similar capacity retention after 100 cycles (Fig. S6). The capacity retention declined to 79.3% (960 mAh g^{-1}) and 74.3% (854 mAh g^{-1})

after 200 cycles, respectively. As expected, the 3D GlM+69.7 wt %S sample showed a sharp degradation in capacity with the increase in the cycle number. Moreover, the Coulombic efficiencies of 3D GlM/S nanocomposites and 3D GlM+69.7 wt%S sample were given in Fig. S7. The three 3D GlM/S nanocomposites showed average Coulombic efficiencies of 97% (43.6 wt%S), 95% (62.8 wt%S) and 94% (72.3 wt%S) at a rate of 0.5 C, repectively. The decrease of the average Coulombic efficiencies with increased sulfur content, maybe due to that the interior micropores and small mesopores (2-7 nm) of 3D GlM have no enough capacity to confine the large amount of elemental sulfur and subsequent lithium polysulfides during the charge/discharge process, thus leading to that the phenomenon of the polysulfide dissolution and shuttling in the electrolytes are more easier to happen when more sulfur is incorporated into the micropores and small mesopores (2-7 nm) in 3D GlM. For comparison, the 3D GlM+69.7 wt%S sample only exhibited a average Coulombic efficiencies of 85%. In addition, we compared the electrochemical performances of the Li-S batteries based on the 3D GlM/S nanocomposites with other typical graphene-sulfur composite materials, as listed in Table S2. The 3D GlM/S nanocomposite is superior to those reported graphene-sulfur composite materials. Therefore, the 3D GlM/S nanocomposites are promising for the practical large-scale application as cathode materials. At higher discharge rates up to 3 C, the 3D GlM/S nanocomposites (43.6 and 72.3 wt %S) displayed excellent rate performances (Fig. S8).

From the above results, we know, the electrochemical performances were gradually decrease with increased sulfur content, which may be related to the microporous and mesoporous volume after sulfur encapsulation. When a low sulfur content of 43.6 wt % was infiltrated into the 3D GlM, the micro- and mesopores of 3D GlM were partly filled, thus remaining large amount of micro- and mesopores, as demonstrsted by the nitrogen adsorption/desorption experiments (Fig. 3 and Table S1). Therefore, the 3D GlM/S nanocomposite (43.6 wt %S) can stably trap the elemental sulfur and, subsequently, the lithium polysulfides during the charge/discharge process, giving a good electrochemical performance. When a high sulfur content of 62.8 wt %, even higher sulfur content of 72.3 wt % were infiltrated, the micro- and mesopores of 3D GlM were largely filled, even fully filled (Fig. 3 and Table S1), thus the 3D GlM/S nanocomposite (62.8 wt %S), especially, the 3D GlM/S nanocomposite (72.3 wt %S) have no enough capacity to confine these large amount of sulfur and lithium polysulfides during the charge/discharge process, thus showing relatively lower capacities and cycle performances.

Based on the excellent overall electrochemical behavior of 3D GlM/S nanocomposites, the hierarchical porous structure and good electrical conductivity of 3D GlM play key role in electrochemical performance. Firstly, the hierarchical porous structure of 3D GlM contains abundant micro- and mesopores, which can provide large total pore volume (large surface area) to maximize the loading of sulfur (can reach up to 72.3 wt%S or more) sequestered by 3D GlM. Secondly, the interconnected micro-, mesopores, and sub-micrometer sized macropores can provide appropriate surfaces and channels to facilitate the sulfur into the interior micro- and mesoporous walls, and preserve fast transport of lithium ions to the sequestered sulfur by ensuring good electrolyte penetration, Thirdly, the 3D porous structure can accommodate the polysulfide in interior pores to minimize lithium polysulfide dissolution and shuttling in the electrolyte, which can enhance the utilization of sulfur to improve the cycle life, and they can also provide stable frame-work to sustain the strain generated by the volume changes of the active material during cycling. The last but not least, the graphene-like structure can provide excellent electronic conductivity to facilitate good transport of electrons from the poorly conducted sulfur.

In summary, a novel 3D GlM/S nanocomposite has been successfully synthesized. The results demonstrated that the 3D GlM is a promising candidate for Li-S batteries. Such 3D GlM, combining ultrahigh specific surface area (2700 m^2 g^{-1}), high conductivity (~1224 S m^{-1}), large pore volume (2.50 cm^3 g^{-1}) and suitable hierarchical porous structure can effectively encapsulate a substantial amount of sulfur and suppress the diffusion of dissolved polysulfides at the same time. Additionally, the 3D GlM/S nanocomposities keep the similar electronic conductivities as that of the pristine 3D GlM to facilitate good transport of electrons from the poor conducting sulfur and remain pores to provide sufficient volume for sulfur expansion and transport of Li^+. As a result, the 3D GlM/S nanocompositie (43.6 wt %S) showed a high stable capacity up to 1067 mAh g^{-1} after 300 cycles at a discharge rate of 0.5 C. The higher sulfur loading 3D GlM/S nanocompositie up to 72.3 wt %S is possible and such high sulfur loading material remained an 854 mAh g^{-1} performance at 0.5 C after 200 cycles. Such highly stable C/S nanocompositie benefited from the three-dimensional graphene-like material with hierarchical pores. It is in evidence that this material could be a promising sulfur cathode for practical and large-scale application in Li-S battery.

Acknowledgments

This work was supported by the Link Project of the National Natural Science Foundation of China and Guangdong Province (U1034003), the Major International (Regional) Joint Research Project (51210002) and the National Natural Science Foundation of China (21073241). Y. Y. Li thanks the Sun Yat-Sen Innovative Talents Cultivation Program for Doctoral Graduate Student.

Notes and references

State Key Laboratory of Optoelectronic Materials and Technologies, and Key Laboratory of Low-carbon Chemistry & Energy Conservation of Guangdong Province, School of Physics and Engineering, Sun Yat-sen University, 135 Xingang Road, Guangzhou, 510275, PR China. Fax: (+8620)-84036736; Tel: (+8620)-84036736; E-mail: stsspk@mail.sysu.edu.cn

† Experiments details and additional physical characterization available: [details of any supplementary information available should be included here]. See DOI: 10.1039/b000000x/

1 P. G. Bruce, S. A. Freunberger, L. J. Hardwick, J. M. Tarascon, *Nat. Mater.*, 2012, **11**, 19-29.

2 B. Scrosati, J. Hassoun, Y. K. Sun, *Energ. Environ. Sci.*, 2011, **4**, 3287-3295.

3 G. C. Li, G. R. Li, S. H. Ye, X. P. Gao, *Adv. Energy. Mater.* , 2012, **2**, 1238-1245.

4 A. Manthiram, Y. Fu, Y. S. Su, *Acc. Chem. Res.*, 2013, **46**, 1125-1134.

5 X. Ji, K. T. Lee, L. F. Nazar, *Nat. Mater.*, 2009, **8**, 500-506.

6 N. Jayaprakash, J. Shen, S. S. Moganty, A. Corona, L. A. Archer, *Angew. Chem. Int. Ed.*, 2011, **50**, 5904-5908.

7 C. Liang, N. J. Dudney, J. Y. Howe, *Chem. Mater.*, 2009, **21**, 4724-4730.

8 C. Zhang, H. B. Wu, C. Yuan, Z. Guo, X. W. D. Lou, *Angew. Chem.*, 2012, **124**, 9730-9733.

9 Y. V. Mikhaylik, J. R. Akridge, *J. Electrochem. Soc.*, 2004, **151**, A1969-A1976.

10 J. Guo, Z. Yang, Y. Yu, H. D. Abruña, L. A. Archer, *J. Am. Chem. Soc.*, 2013, **135**, 763-767.

11 S. Xin, L. Gu, N. H. Zhao, Y. X. Yin, L. J. Zhou, Y. G. Guo, L. J. Wan, *J. Am. Chem.Soc.*, 2012, **134**, 18510-18513.

12 B. Rao, J. Shropshire, *J. Electrochem. Soc.*, 1981, **128**, 942-945.

13 K. T. Lee, R. Black, T. Yim, X. Ji, L. F. Nazar, *Adv. Energy Mater.*, 2012, **2**, 1490-1496.

14 L. Xiao, Y. Cao, J. Xiao, B. Schwenzer, M. H. Engelhard, L. V. Saraf, Z. Nie, G. J. Exarhos, J. Liu, *Adv. Mater.*, 2012, **24**, 1176-1181.

15 G. Y. Zheng, Y. Yang, J. J. Cha, S. S. Hong, Y. Cui, *Nano. Lett.*, 2011, **11**, 4462-4467.

16 S. Evers, L. F. Nazar, *Acc. Chem. Res.*, 2012, **46**, 1135-1143.

17 X. Tao, X. Chen, Y. Xia, H. Huang, Y. Gan, R. Wu, F. Chen, *J. Mater. Chem. A*, 2013, **1**, 3295-3301.

18 J. C. Guo, Z. C. Yang, Y. C. Yu, H. c. D. Abruña, L. A. Archer, *J. Am. Chem. Soc.*, 2012, **135**, 763-767.

19 B. Zhang, X. Qin, G. Li, X. Gao, *Energ. Environ. Sci.*, 2010, **3**, 1531-1537.

20 Y. S. Su, A. Manthiram, *Nat. Commun.*, 2012, **3**, 1166.

21 J. Schuster, G. He, B. Mandlmeier, T. Yim, K. T. Lee, T. Bein, L. F. Nazar, *Angew. Chem. Int. Ed.*, 2012, **51**, 3591-3595.

22 R. Elazari, G. Salitra, A. Garsuch, A. Panchenko, D. Aurbach, *Adv. Mater.*, 2011, **23**, 5641-5644.

23 H. Wang, Y. Yang, Y. Liang, J. T. Robinson, Y. Li, A. Jackson, Y. Cui, H. Dai, *Nano. Lett.*, 2011, **11**, 2644-2647.

24 L. Ji, M. Rao, H. Zheng, L. Zhang, Y. Li, W. Duan, J. Guo, E. J. Cairns, Y. Zhang, *J. Am. Chem. Soc.*, 2011, **133**, 18522-18525.

25 D. Wang, Q. Zeng, G. Zhou, L. Yin, F. Li, H. M. Cheng, I. Gentle, G. Q. Lu, *J. Mater. Chem. A*, 2013, **1**, 9382 -9394.

26 G. M. Zhou, L. C. Yin, D. W. Wang, L. Li, S. F. Pei, I. R. Gentle, F. Li, H. M. Cheng, *ACS. Nano.*, 2013, **7**, 5367-5375.

27 B. Ding, C. Z. Yuan, L. F. Shen, G. Y. Xu, P. Nie, Q. X. Lai, X. G. Zhang, *J. Mater. Chem. A*, 2013, **1**, 1096-1101.

28 Z. K. Wei, J. J. Chen, L. L. Qin, A. W. Nemage, M. S. Zheng, Q. F. Dong, *J. Electrochem. Soc.*, 2012, **159**, A1236-A1239.

29 J. Jin, Z. Y. Wen, G. Q. Ma, Y. Lu, Y. M. Cui, M. F. Wu, X. Liang, X. W. Wu, *RSC Adv.*, 2013, **3**, 2558-2560.

30 J. Q. Huang, X. F. Liu, Q. Zhang, C. M. Chen, M. Q. Zhao, S. M. Zhang, W. C. Zhu, W. Z. Qian, F. Wei, *Nano Energy*, 2012, **2**, 314-321.

31 C. Li, G. Q. Shi, *Nanoscale*, 2012, **4**, 5549-5563.

32 X. Wan, Y. Huang, Y. Chen, *Acc. Chem. Res.*, 2012, **45**, 598-607.

33 S. Nardecchia, D. Carriazo, M. L. Ferrer, M. C. Gutiérrez, F. del Monte, *Chem. Soc. Rev.*, 2013, **42**, 794-830.

34 K. S. Kim, Y. Zhao, H. Jang, S. Y. Lee, J. M. Kim, K. S. Kim, J. H. Ahn, P. Kim, J. Y. Choi, B. H. Hong, *Nature*, 2009, **457**, 706-710.

35 Z. Chen, W. Ren, L. Gao, B. Liu, S. Pei, H.-M. Cheng, *Nat. Mater.*, 2011, **10**, 424-428.

36 X. Y. Xiao, T. E. Beechem, M. T. Brumbach, T. N. Lambert, D. J. Davis, J. R. Michael, C. M. Washburn, J. Wang, S. M. Brozik, D. R. Wheeler, *ACS. Nano.*, 2012, **6**, 3573-3579.

37 Z. Ryu, J. Zheng, M. Wang, B. Zhang, *Carbon*, 1999, **37**, 1257-1264.

38 Y. W. Zhu, S. Murali, M. D. Stoller, K. J. Ganesh, W. W. Cai, P. J. Ferreira, A. Pirkle, R. M. Wallace, K. A. Cychosz, M. Thommes, D. Su, E. A. Stach, R. S. Ruoff, *Science*, 2011, **332**, 1537-1541.

39 C. Barchasz, F. Molton, C. Duboc, J.-C. Leprêtre, S. Patoux, F. Alloin, *Anal. Chem.*, 2012, **84**, 3973-3980.

40 J. Kim, D. J. Lee, H. G. Jung, Y. K. Sun, J. Hassoun, B. Scrosati, *Adv. Funct. Mater.*, 2013, **23**, 1076-1080.

41 B. Ding, C. Yuan, L. Shen, G. Xu, P. Nie, X. Zhang, *Chem. Eur. J.*, 2013, **19**, 1013-1019.

42 J. Z. Wang, L. Lu, M. Choucair, J. A. Stride, X. Xu, H. K. Liu, *J. Power Sources*, 2011, **196**, 7030-7034.

43 Y. Yang, G. Yu, J. J. Cha, H. Wu, M. Vosgueritchian, Y. Yao, Z. Bao, Y. Cui, *ACS. Nano.*, 2011, **5**, 9187-9193.

44 S. W. Oh, S. T. Myung, S. M. Oh, K. H. Oh, K. Amine, B. Scrosati, Y. K. Sun, *Adv. Mater.*, 2010, **22**, 4842-4845.

45 K. Saravanan, P. Balaya, M. Reddy, B. Chowdari, J. J. Vittal, *Energ. Environ. Sci.*, 2010, **3**, 457-463.

46 X. M. Lou, Y. X. Zhang, *J. Mater. Chem.*, 2011, **21**, 4156-4160.

47 J. Y. Luo, H. M. Xiong, Y. Y. Xia, *J.Phys. Chem. C*, 2008, **112**, 12051-12057.

48 H. Y. Xu, B. Cheng, Y. P. Wang, L. Zheng, X. H. Duan, L. H. Wang, J. Yang, Y. T. Qian, *Int. J. Electrochem. Sci.*, 2012, **7**, 10627-10632.

49 H. J. Yue, X. K. Huang, D. P. Lv, Y. Yang, *Electrochimica Acta*, 2009, **54**, 5363-5367.

50 S. Luo, K. Wang, J. P. Wang, K. L. Jiang, Q. Q. Li, S. S. Fan, *Adv. Mater.*, 2012, **24**, 2294-2298.

51 Y. S. Jung, A. S. Cavanagh, A. C. Dillon, M. D. Groner, S. M. George, S. H. Lee, *J. Electrochem. Soc.*, 2010, **157**, A75-A81.

52 I. D. Scott, Y. S. Jung, A. S. Cavanagh, Y. Yan, A. C. Dillon, S. M. George, S. H. Lee, *Nano. Lett.*, 2010, **11**, 414-418.

Entry for the Table of Contents

A rational design and synthesis of sulphur-carbon nanocomposites by infiltrating into 3D graphene-like material (GlM) with hierarchical pores has been achieved for the first time and such 3D GlM/S nanocomposite shows a highly stable capacity and reversible high rate charge/discharge performance.